10-26-2021

Hydrogen/Deuterium Exchange Measurements May Provide an Incomplete View of Protein Dynamics: a Case Study on Cytochrome

Pablo M Scrosati

Victor Yin

Lars Konermann

Hydrogen/Deuterium Exchange Measurements May Provide an Incomplete View of Protein Dynamics: A Case Study on Cytochrome *c*

Pablo M. Scrosati, Victor Yin, and Lars Konermann*

Department of Chemistry, The University of Western Ontario, London, Ontario N6A 5B7, Canada

* corresponding author: konerman@uwo.ca

Funding was provided by the Natural Sciences and Engineering Research Council of Canada (RGPIN-2018-04243).

ABSTRACT: Many aspects of protein function rely on conformational fluctuations. Hydrogen/deuterium exchange (HDX) mass spectrometry (MS) provides a window into these dynamics. Despite the widespread use of HDX-MS, it remains unclear whether this technique provides a truly comprehensive view of protein dynamics. HDX is mediated by H-bond opening/closing events, implying that HDX methods provide a H-bond-centric view. This raises the question if there could be fluctuations that leave the H-bond network unaffected, thereby rendering them undetectable by HDX-MS. We explore this issue in experiments on cytochrome *c* (cyt *c*). Compared to the Fe(II) protein, Fe(III) cyt *c* shows enhanced deuteration on both the distal and proximal sides of the heme. Previous studies have attributed enhanced dynamics of Fe(III) cyt *c* to the facile and reversible rupture of the distal M80-Fe(III) bond. Using molecular dynamics (MD) simulations, we conducted a detailed analysis of various cyt *c* conformers. Our MD data confirm that rupture of the M80-Fe(III) contact triggers major reorientation of the distal Ω loop. Surprisingly, this event takes place with only miniscule H-bonding alterations. In other words, the distal loop dynamics are almost "HDX-silent". Moreover, distal loop movements cannot account for enhanced dynamics on the opposite (proximal) side of the heme. Instead, enhanced deuteration of Fe(III) cyt *c* is attributed to sparsely populated conformers where both the distal (M80) and the proximal (H18) coordination bonds have been ruptured, along with opening of numerous H-bonds on both sides of the heme. We conclude that there can be major structural fluctuations that are only weakly coupled to changes in H-bonding, making them virtually impossible to track by HDX-MS. In such cases, HDX-MS may provide an incomplete view of protein dynamics.

Introduction

Proteins in solution continuously sample their conformational space via random fluctuations.[1] The occupancy of each conformer is determined by its free energy.[2] Fluctuations between the native ground state and alternative conformations are believed to mediate enzyme catalysis, [3-6] allosteric regulation,[7-10] ligand binding,[11, 12] aggregation,[13] degradation,[14] etc. However, details of these dynamics-function relationships remain poorly understood. Advances in this area require techniques that can track protein dynamics over a wide range of time scales.[15, 16] Hydrogen-deuterium exchange (HDX) methods are a key tool in this context. These experiments monitor backbone NH $\rightarrow$ ND conversion in D_2O labeling buffer. Early HDX investigations used NMR spectroscopy.[17] Today, most HDX studies rely on mass spectrometry (MS) which offers higher sensitivity and can be applied to proteins beyond the NMR size range. HDX-MS is being used for numerous applications, from fundamental biophysics to the characterization of protein drugs. Most HDX-MS studies are conducted in a comparative fashion by examining a protein under different conditions, e.g., unmodified vs. chemically altered.[2, 4, 6, 18-29]

According to the well-accepted Linderstrøm-Lang model,[2, 30, 31] HDX is mediated by H-bond fluctuations between a closed NH···OC state, and an open state where the H-bond is disrupted. OD^--catalyzed deuteration of NH_{OPEN} proceeds with the "chemical" rate constant k_{ch}.[2]

$$\mathrm{NH_{CLOSED}} \underset{k_{cl}}{\overset{k_{op}}{\rightleftarrows}} \mathrm{NH_{OPEN}} \xrightarrow{k_{ch}} \mathrm{ND} \qquad (1)$$

HDX for most native proteins proceeds in the EX2 limit ($k_{cl} >> k_{ch}$) where each NH visits the open state numerous times before it is deuterated, resulting in a HDX rate constant $k_{HDX} = K_{op}\, k_{ch}$, with $K_{op} = k_{op}/k_{cl}$.[2, 32] Under EX2 conditions, the opening/closing frequency does not affect k_{HDX}, as long as K_{op} remains constant.[2, 32] Opening/closing in eq. 1 involves short-lived unfolding/refolding

transitions that can represent local, sub-global, or global events.[2, 30, 33] Protein regions that undergo fast deuteration (large K_{op}) are considered to be "dynamic", while slow deuteration (small K_{op}) signifies "rigid" elements.[2, 4, 6, 18-29] The very low equilibrium populations of NH_{OPEN} conformers are undetectable by conventional methods, where signals are dominated by the native state.[2]

A question that has received surprisingly little attention is the following: Does HDX-detected H-bond opening/closing provide a *comprehensive* view of protein dynamics? We posit that there could be dynamic events that are not associated with $NH_{CLOSED} \leftrightarrow NH_{OPEN}$ fluctuations. The detection of such dynamics by HDX methods would be impossible, according to eq.1. Examples of such "HDX-silent" dynamics could include rigid body domain movements, and some motions of motor proteins.[28, 34-36] Also, proteins crystallized in different conformations (that represent interconverting solution structures) often show similar H-bonding.[12, 36, 37] This tendency to avoid NH_{OPEN} sites reflects the large thermodynamic penalty ($\Delta G \approx$ 2-6 kJ mol^{-1}) associated with opening of each H-bond.[38] We do not dispute that proteins transiently visit partially unfolded states, in accordance with the foldon model.[2, 39] Such fluctuations involve H-bond opening/closing, rendering them detectable by HDX methods. Our point is that there may be additional dynamics that are orthogonal to these $NH_{CLOSED} \leftrightarrow NH_{OPEN}$ fluctuations, e.g., transitions between different folded structures.[1] Hence, an interpretation of protein dynamics solely in the context of H-bond opening/closing (as often implied in the HDX literature) may be too restrictive.

Here we explore the possible occurrence of dynamics that are not (or only weakly) coupled to H-bond opening/closing. We focus on cytochrome *c* (cyt *c*), a protein that has previously been used for studying the connection between HDX and conformational dynamics.[2, 39, 40] The globular structure of cyt *c* is folded around a covalently bound heme.[41] X-ray data show the heme iron in a 6-coordinate environment. M80 is the distal ligand, H18 is the proximal ligand, and the four

remaining contacts are provided by porphyrin nitrogens.[41] Cyt *c* acts as mitochondrial electron carrier by switching between the Fe(II) and Fe(III) states. In addition, cyt *c* has attracted major attention because it can turn into an apoptotic peroxidase.[37, 42, 43] Alternative heme ligation scenarios can become populated after covalent modifications or environmental changes. Many of these alternative structures affect the distal side of the heme, facilitated by the malleability of the distal M80-containing 71-85 Ω loop.[2, 43-47]

Fe(III) and Fe(II) cyt *c* share virtually the same native structure, but Fe(III) cyt *c* is less stable and more dynamic than the Fe(II) state.[40, 48-51] These differences have been attributed to the M80-Fe bond,[52, 53] which is only half as strong for the Fe(III) state.[49] The M80-Fe(III) contact can be ruptured by photo-excitation,[54] denaturants,[2] ligand binding,[42, 55-57] and pH changes.[42] Even under native conditions, the M80-Fe(III) bond undergoes transient dissociation, causing 6-coordinate native cyt *c* to sporadically visit a 5-coordinate state.[2, 49, 55] Additionally, 4-coordinate structures (lacking both the M80 and H18 bonds) can exist under certain conditions.[54, 58-61]

The current work uses HDX-MS and molecular dynamics (MD) simulations to probe differences between Fe(II) and Fe(III) cyt *c*. The Fe(III) protein shows enhanced HDX in two well-defined regions, indicating that NH_{OPEN} sites become more strongly populated in these segments upon Fe oxidation. Surprisingly, we find that enhanced fluctuations between 6- and 5-coordinate structures *cannot* account for the elevated deuteration of Fe(III) cyt *c*. Instead, the HDX differences are attributed to dynamics involving a sparsely populated 4-coordinate conformer. The more prevalent 6 ↔ 5-coordinate dynamics are nearly HDX-silent. These findings illustrate that proteins can undergo large-scale dynamic events that only minimally influence experimental HDX patterns.

Materials and Methods

Equine cyt *c* was purchased from Sigma (St. Louis, MO). Fe(III) protein was produced by exposure to the oxidizing agent potassium ferricyanide, while Fe(II) cyt *c* was prepared using the reducing agent sodium ascorbate. HDX-MS followed a standard workflow on a nanoACQUITY HDX/UPLC (Waters, Milford, MA) that was coupled to a Synapt G2-Si Q-TOF. All-atom μs MD simulations were conducted using GROMACS 2020.3,[62] with the CHARMM36 force field[63] and TIP3P water. Complete experimental and computational details are provided in the SI.

Results and Discussion

HDX Behavior of Fe(II) and Fe(III) Cyt *c*. Incubation in D_2O labeling buffer caused progressive deuteration of cyt *c* (Figure 1). In agreement with earlier experiments,[48] HDX under the conditions used here took place under EX2 conditions. A number of peptides showed kinetics that were virtually indistinguishable for the Fe(II) and Fe(III) states; these peptides were found in the N-terminal (1-30) and the C-terminal regions (81-104). In contrast, peptides closer to the center of the sequence (residues 31 to 80) underwent significantly higher deuteration in Fe(III) cyt *c* than in the Fe(II) state. Deuteration patterns very similar to those shown in Figure 1 have been reported in earlier HDX investigations on Fe(II) and Fe(III) cyt *c*.[48, 64] Overall, our observations support the view that Fe(III) cyt *c* is more dynamic than the Fe(II) state.[40, 48-52]

To visualize the deuteration differences between Fe(II) and Fe(III) cyt *c*, we superimposed a colored HDX difference map onto the X-ray coordinates of the native protein (Figure 2). The 10 min time point was selected for this purpose because it exhibited the largest difference between the two oxidation states. Red coloring in Figure 2 denotes segments that were more highly

deuterated in the Fe(III) state than in Fe(II) cyt *c*. There were two distinct regions of strongly enhanced deuteration; one was on the distal side ("above" the heme in Figure 2), comprising the 60s helix as well as most of the 71-85 Ω loop with the M80 heme ligand. The second region of enhanced deuteration was on the proximal side ("below" the heme in Figure 2). This second region covers residues 24 to 45, stretching across parts of the 18-36 and 40-57 Ω loops that are in tertiary contact with the H18 heme ligand. When interpreting the data of Figure 2 in the context of eq. 1, one can conclude that the Fe(II) → Fe(III) transition shifts $NH_{CLOSED} \leftrightarrow NH_{OPEN}$ equilibria on both the distal and the proximal side of the heme more toward the open state.

Possible Mechanisms for the HDX Enhancements in Fe(III) Cyt *c*. The more dynamic nature and lower stability of Fe(III) cyt *c* relative to the Fe(II) protein[40, 48-51, 64] have been attributed to weakening of the distal coordination bond, with transient rupture of the M80-Fe(III) contact.[49, 52, 53] This contact acts as an anchor for the tertiary packing of the distal segments.[2] It is therefore easy to imagine how transient rupture of the M80-Fe(III) bond could destabilize H-bonds in the distal region.[48] However, it is difficult to rationalize why the weakened M80-Fe(III) bond would also boost HDX on the opposite side of the heme ("red" proximal elements, below the heme in Figure 2). Two different scenarios could explain the observed HDX pattern.

(*i*) An allosteric mechanism could propagate distal protein destabilization into proximal regions. Similar allosteric signal transmission processes have been demonstrated for other proteins.[7-10] (*ii*) Alternatively, the Fe(II) → Fe(III) transition may cause destabilization of *both* coordination bonds, allowing transient rupture of the distal M80-Fe(III) contact as well as the proximal Fe(III)-H18 bond. It is known that the Fe-His bond can be severed, i.e., in denaturing solutions[58-60] and after photo-excitation,[54, 61] resulting in a 4-coordinate iron center. Therefore, Fe-

H18 bond cleavage may occur even under native conditions, albeit transiently and with a low Boltzmann probability. Thus, in addition to the well documented fluctuations between 6-coordinate and 5-coordinate cyt *c*,[2, 49, 55] there could be rare instances of 4-coordinate Fe(III) conformers.[54, 58-61] Rupture of coordination bonds on both sides of heme could then trigger distal as well as proximal H-bond opening. From the subsequent data it will be seen that scenario (*i*) is not tenable. Instead, the results discussed below strongly support scenario (*ii*), i.e., the involvement of sparsely populated 4-coordinate species.

MD Simulations of Cyt *c*. To uncover the origin of the distal/proximal HDX enhancement in Fe(III) cyt *c*, we performed atomistic μs MD simulations in explicit water. Such simulations have become an important complementary tool for HDX studies.[23, 31, 33, 65-68] This is despite the fact that some HDX-relevant $NH_{CLOSED} \leftrightarrow NH_{OPEN}$ fluctuations are rare events, making them difficult to observe on MD-accessible time scales.[33, 65, 68] One way to address this problem is by extending MD time windows as much as possible.[33, 69] Unfortunately, even the longest simulations (milliseconds) are orders of magnitude shorter than typical HDX labeling times (seconds to hours).

Here we circumvented the MD time scale problem using a different strategy. As noted, the key difference between Fe(II) and Fe(III) cyt *c* is the occasional dissociation of the M80-Fe(III) bond and possibly also the Fe(III)-H18 contact. Instead of trying to spontaneously generate these rare 5- and 4-coordinate states in long simulations, we modeled them directly by severing the corresponding Fe(III) bonds. In this way we could test whether the H-bonding properties of these sparsely populated species can explain the experimentally observed HDX patterns.

For our targeted MD approach we modeled four species. (A) "*Native Fe(II) cyt c*" has a 6-coordinate M80-Fe(II)-H18 heme. It served as MD reference state, analogous to our HDX

experiments. (B) "*6-coordinate Fe(III) cyt c*" has a M80-Fe(III)-H18 geometry and represents the ground state of the oxidized protein. (C) "*5-coordinate Fe(III) cyt c*" is a Fe(III)-H18 species that lacks distal ligation. It is known to exist in equilibrium with 6-coordinate Fe(III) cyt *c* as a result of weakened M80-Fe bonding.[49, 52, 53] (D) "*4-coordinate Fe(III) cyt c*" denotes a fleeting species that has neither M80 nor H18 coordination, as outlined above under scenario (*ii*).[54, 58-61]

MD runs for all four species commenced from the native X-ray structure.[41] Representative MD structures generated in this way are depicted in Figure 3 (see Figure S3 for additional details). In all cases, the proteins retained a compact fold. Native Fe(II) cyt *c* and 6-coordinate Fe(III) cyt *c* were quite similar to each other, with only minor differences in the orientations of Ω loops 18-36 and 40-57 (Figures 3A, S3).

Severing of the M80-Fe contact generated 5-coordinate Fe(III) cyt *c* and allowed the distal 71-85 Ω loop to swing upward, dramatically increasing the S/Fe distance from 0.25 nm to ~0.65 nm (Figure 3B). In some MD runs this transition took place within a few ns, whereas in other instances these events required up to ~100 ns (Figure S3). Except for these Ω loop changes, 5-coordinate Fe(III) cyt *c* had a structure similar to native Fe(II) cyt *c* (Figure 3B). These MD results are in agreement with NMR structural data for 5-coordinate M80A Fe(III) cyt *c*.[70]

Even larger structural changes were seen for 4-coordinate Fe(III) cyt *c*, particularly in the three Ω loops (Figures 3C, S3). The M80-Fe distance increased to around 0.8 nm, while the Fe-H18 distance change was more subtle (from 0.22 nm to 0.31 nm). The vacant distal site on the iron established contact with the Y67 hydroxyl O, reminiscent of some cyt *c* mutants.[71]

Figure 4 compares the three Fe(III) species, with focus on the distal Ω loop (residues 71-85). In 6-coordinate cyt *c* this loop covered the heme, rendering the Fe center inaccessible (Figure 4A). Major repositioning of the distal loop in the 5-coordinate protein resulted in dramatic opening

of the heme binding pocket (Figure 4B). For 4-coordinate Fe(III) cyt *c*, the distal region was once again more collapsed (Figure 4C), making the heme less accessible than in the 5-coordinate state.

H-bond Dynamics. $NH_{CLOSED} \leftrightarrow NH_{OPEN}$ fluctuations were tracked by monitoring H···O distances throughout the MD runs. A 0.25 nm cutoff value commonly serves as criterion for an intact H-bond.[72] However, in an HDX context such a rigid cutoff may not always be meaningful. For example, a H···O distance of 0.26 nm will likely still provide some protection, while this would not be the case for 0.5 nm[33] (both are "open" according to the 0.25 nm cutoff).[72] Keeping with tradition, we will continue to refer to H-bonds as open or closed. However, in addition to this binary classification we will report actual H···O distances (or distance differences) throughout this work, to reflect the fact that H-bond opening is not always an all-or-nothing event.

Figure 5 exemplifies the behavior of four NH sites in 6-coordinate Fe(III) cyt *c*. A96 forms an H-bond that remained permanently closed. I75 displayed a single opening/closing event, with an open state that had a dramatically increased H···O distance of ~0.7 nm. E104 underwent multiple opening/closing cycles, although opening was somewhat less dramatic (~0.4 nm) than in the previous example. F46 spent most of its time in the open state (0.3 to 0.5 nm), while only occasionally dipping below 0.25 nm. It is gratifying that MD simulations can visualize these H-bond dynamics, thereby providing an atomistic underpinning for the Linderstrøm-Lang model (eq. 1).[33, 65, 68]

Overview of H-bonding and Chain Fluctuations. Average H···O bond distances were calculated for NH sites in all four MD species (Figure S4). The center portions of the N-terminal and C-terminal helices retained closed H-bonds in all cases, reflecting the known stability of these

segments.[2] Helix fraying occurred for the first and the last ~6 residues in the sequence, consistent with NMR data.[73]

To facilitate a comparison of the four species, H-bonding patterns from Figure S4 were compiled into difference plots, using native Fe(II) cyt *c* as reference (Figure 6). These plots mirror the "Fe(III) minus Fe(II)" approach taken for the experimental data. Thus, Fe(III) NH sites in Figure 6 can be more open (red) or more closed (blue) than in native Fe(II) cyt *c*. The difference plots can be summarized as follows: 6-coordinate Fe(III) cyt *c* has enhanced H-bonding in roughly a dozen NH sites, while a handful of NH sites exhibit slight opening (Figure 6B). The H-bond pattern of 5-coordinate Fe(III) cyt *c* is surprisingly similar to that of the native Fe(II) protein. The 5-coordinate form underwent H-bond opening only at residues 49-51, as well as closing at 23 and 31. In other words, 5-coordinate Fe(III) cyt *c* did *not* undergo large-scale H-bond opening in the distal or proximal regions (Figure 6C). Dramatic H-bond opening took place only for 4-coordinate Fe(III) cyt *c*, spanning residues 23 to 95 (Figure 6D).

To characterize protein dynamics in more detail, we determined the root mean square fluctuation (RMSF) of each backbone N atom. RMSF(*i*) represents the standard deviation of atomic position *i* relative to its average position, i.e., it measures the extent of conformational fluctuations during the MD time window (Figure S5). RMSF difference plots (Fe(III) minus Fe(II)) are included in Figure 6. According to these ΔRMSF data, 6-coordinate Fe(III) cyt *c* is less dynamic than the native Fe(II) protein in the 41 to 55 range, while all other residues were virtually indistinguishable from the Fe(II) state (Figure 6B). Differences between 5-coordinate Fe(III)-H18 cyt *c* and the Fe(II) reference were small, with only slightly elevated dynamics around M80 (Figure 6C). This is despite the fact that the distal loop undergoes a major reorientation upon forming the 5-coordinate state (green arrow in Figure 4B). The relatively small ΔRMSF of the distal loop

(Figure 6C) implies that this region maintains a fairly stable structure following the initial reorientation event, instead of continuing to undergo major fluctuations during the MD time window. Large positive ΔRMSF values were seen only for 4-coordinate Fe(III) cyt *c*, identifying it as the most dynamic species (Figure 6D). By and large, the ΔRMSF data in Figure 6 mirror the H-bond behavior, i.e., highly dynamic regions (with large RMSFs) tend to be correlated with H-bond opening, particularly for 4-coordinate Fe(III) cyt *c* (Figure 6D). One region that seemingly does not follow this trend is centered around G45, where Figure 6D shows large ΔRMSFs with only minor changes in H-bonding. This behavior reflects the fact that most NH sites around G45 are already open in the Fe(II) reference state (Figure S4).

Linking HDX and MD Data. Our experiments showed strongly enhanced distal and proximal deuteration for Fe(III) cyt *c* compared to the Fe(II) protein. According to eq. 1, this implies that for Fe(III) cyt *c* the corresponding residues spend more time in the NH_{OPEN} state. What is the origin of this enhanced H-bond opening? This question can be answered by comparing experimental data (summarized in Figure 6A) with H-bond patterns of the various MD structures (Figure 6B-D).

There is no resemblance between the experimental HDX data and the MD-predicted H-bond pattern of 6-coordinate Fe(III) cyt *c*. On the contrary, the 6-coordinate MD structure showed stronger H-bonding for numerous residues compared to its Fe(II) counterpart (Figure 6B). Thus, the 6-coordinate Fe(III) state of Figure 6B would cause a decrease in HDX, which is opposite to the experimentally observed behavior. These findings demonstrate that oxidation to Fe(III) *per se* does not promote H-bond opening.

It is well known that Fe(III) cyt *c* fluctuates between the 6-coordinate ground state and 5-coordinate structures,[49, 52, 53, 55] facilitated by the relatively weak M80-Fe(III) bond.[40, 48-51]

Surprisingly, these 6 ↔ 5-coordinate fluctuations are *not* coupled to large-scale NH_{CLOSED} ↔ NH_{OPEN} transitions (Figure 6C). The 5-coordinate protein showed H-bond opening only for a few residues (49-51). Most distal and proximal H-bonds remained largely unaffected. This NH_{OPEN} pattern bears no resemblance to the experimental opening of Figure 6A. Because fluctuations between 6- and 5-coordinate cyt *c* fail to significantly boost deuteration of Fe(III) cyt *c*, the allosteric "scenario (*i*)" that we considered earlier must be ruled out.

Evidence supports the existence of 4-coordinate Fe(III) cyt *c* as a fleeting species with an equilibrium population even lower than that of the 5-coordinate protein.[54, 58-61] Our data show that this 4-coordinate species represents the missing piece of the puzzle. The 4-coordinate protein possesses multiple open H-bonds, particularly for proximal and distal residues (Figure 6D). This opening pattern most closely matches the experimental data of Figure 6A.

It would be unrealistic to expect that the MD simulations *exactly* match our experiments, especially when keeping in mind the different nature of the data (single residue vs. peptide-resolved). For example, the simulations predict that proximal H-bond opening starts at residue 23 (Figure 6D), whereas experiments indicate that this deprotection commences somewhat later, around residue 30 (see peptides 19-30 and 24-36, Figure 1). Similarly, Figure 6D shows increased opening around residues 3-4, an effect that is not mirrored in the experimental data (Figure 6A). We attribute this behavior to the fact that the first few residues are quite dynamic in the Fe(II) state (note their large error bars in Figure S4A), such that further opening of this region in 4-coordinate Fe(III) cyt *c* will not significantly enhance deuteration. Such relatively minor issues should not deter from the fact that the MD data of Figure 6D match the experimental pattern of Figure 6A quite well. This is in contrast to Figures 6B & C, which bear no resemblance to Figure 6A.

In summary, our data imply that 6-coordinate Fe(III) cyt *c* undergoes transient fluctuations to a 5-coordinate structure (with rupture of the M80 contact), as well as rare transitions to a 4-coordinate species (with additional rupture of the H18 contact). Only the 4-coordinate species exhibits a wide range of NH_{OPEN} sites, thereby accounting for the experimentally observed distal and proximal HDX enhancement. The 5-coordinate protein contributes very little to this HDX enhancement because of its low number of NH_{OPEN} sites.

The sparsely populated 5- and 4-coordinate Fe(III) states are undetectable in traditional spectroscopic experiments, where signals are dominated by the 6-coordinate ground state. HDX methods are unique in this regard, because they report on rare excursions to NH_{OPEN} conformers that have very low Boltzmann probabilities.[2, 4, 6, 18-28] In summary, Fe(III) cyt *c* shows enhanced HDX compared to the Fe(II) protein, because 4-coordinate conformers are more highly populated in the Fe(III) state, as dictated by its weaker coordination bonds.[40, 48-51] These findings are in line with "scenario (*ii*)" that we outlined above.

Conclusions

The Linderstrøm-Lang model asserts that H-bond opening/closing is a prerequisite for HDX.[2, 30, 31] Protein dynamics that are not associated with H-bond opening/closing are therefore undetectable by HDX methods. Figures 7A and 7B schematically illustrate this issue for fluctuations between a native ground state and an alternative conformer that has a higher free energy. The diagonal transition of Figure 7A is HDX-detectable because it entails H-bond opening. In contrast, the vertical transition of Figure 7B is HDX-silent.

The possible existence of HDX-silent dynamics has received very little attention in the literature. HDX practitioners tend to make the implicit assumption that deuteration provides a

rather comprehensive view of protein dynamics. Here we point out that this assumption may not always be warranted. Fluctuations between 6- and 5-coordinate forms are highly prevalent in Fe(III) cyt *c*.[40, 49-52, 64] These fluctuations are of major functional significance because they expose the distal side of the heme, representing the first step of an activation cascade that turns cyt *c* into an apoptotic peroxidase.[43] However, these distal fluctuations are only weakly coupled to H-bond opening/closing, rendering them almost HDX-silent. Instead, our MD simulations strongly suggest that the HDX difference data are governed by rare fluctuations to a 4-coordinate state (Figure 7C).

This work is *not* an attempt to topple the foldon model, according to which the cyt *c* HDX behavior is governed by fluctuations between conformers that are unfolded to different degrees.[2, 39] Instead, our data complement the foldon model. We propose that certain fluctuations (highlighted in Figure 7C) are selectively enhanced in Fe(III) cyt *c*, and that these fluctuations occur on top of the previously described foldon dynamics.[2, 39] Foldon energy level diagrams aim to account for the deuteration of *all* NH sites in a protein.[2, 39] In contrast, Figure 7C only refers to a *subset* of NH sites that exchange faster in the Fe(III) protein, identified via comparison with Fe(II) cyt *c*.

Protein dynamics comprise a wide range of motions. Many of these motions are strongly coupled to H-bond opening/closing, while for others this coupling may be weaker. The latter will be difficult to detect by HDX methods. We do *not* dispute that HDX methods are a powerful tool for interrogating protein dynamics, and we do *not* imply that HDX data are flawed in any way. Rather, we point out that any analytical technique has its limitations. For example, Raman spectroscopy is widely used for probing molecular vibrations. However, only certain vibrations cause Raman scattering, whereas others are "Raman-silent". Thus, Raman spectroscopy may provide an incomplete view of molecular vibrations.[74] Analogously, we point out that some protein

motions can be HDX-silent, such that HDX-MS may provide an incomplete view of protein dynamics.

While the current investigation only examined cyt *c*, previous data suggest that HDX-silent dynamics also occur in other proteins.[28, 34-36] However, this work marks the first time that such a scenario has been examined in detail. In future studies it will be interesting to see how widespread HDX-silent dynamics are. In any case, it is hoped that our work will help to more clearly define the strengths and limitations of HDX methods as a tool for deciphering the protein structure/dynamics/function triad.

Supporting Information: Complete Methods Section, Figure S1: UV-Vis and MS characterization of cyt *c* samples, Figure S2: HDX sequence coverage, Figure S3: Time dependence of various interatomic distances during MD runs, Figure S4: Dynamic H-bond patterns of different cyt *c* conformers, Figure S5: Summary of backbone nitrogen RMSF values. DynamX-generated kinetic data.[27]

References

(1) Frauenfelder, H.; Sligar, S. G.; Wolynes, P. G. The Energy Landscape and Motions of Proteins. *Science* **1991**, 254, 1598-1603.

(2) Englander, S. W.; Mayne, L.; Kan, Z. Y.; Hu, W. B. Protein Folding-How and Why: By Hydrogen Exchange, Fragment Separation, and Mass Spectrometry. *Annu. Rev. Biophys.* **2016**, 45, 135-152.

(3) Liang, Z.-X.; Lee, T.; Resing, K. A.; Ahn, N. G.; Klinman, J. P. Thermal-activated protein mobility and its correlation with catalysis in thermophilic alcohol dehydrogenase. *Proc. Natl. Acad. Sci. U.S.A.* **2004**, 101, 9556-9561.

(4) Liuni, P.; Jeganathan, A.; Wilson, D. J. Conformer Selection and Intensified Dynamics During Catalytic Turnover in Chymotrypsin. *Angew. Chem. Int. Ed.* **2012**, 51, 9666 –9669.

(5) Bhabha, G.; Lee, J.; Ekiert, D. C.; Gam, J.; Wilson, I. A.; Dyson, H. J.; Benkovic, S. J.; Wright, P. E. A Dynamic Knockout Reveals That Conformational Fluctuations Influence the Chemical Step of Enzyme Catalysis. *Science* **2011**, 332, 234-238.

(6) Thompson, E. J.; Paul, A.; Iavarone, A. T.; Klinman, J. P. Identification of Thermal Conduits That Link the Protein-Water Interface to the Active Site Loop and Catalytic Base in Enolase. *J. Am. Chem. Soc.* **2021**, 143, 785-797.

(7) Deredge, D.; Li, J. W.; Johnson, K. A.; Wintrode, P. L. Hydrogen/Deuterium Exchange Kinetics Demonstrate Long Range Allosteric Effects of Thumb Site 2 Inhibitors of Hepatitis C Viral RNA-dependent RNA Polymerase. *J. Biol. Chem.* **2016**, 291, 10078-10088.

(8) Underbakke, E. S.; Iavarone, A. T.; Chalmers, M. J.; Pascal, B. D.; Novick, S.; Griffin, P. R.; Marletta, M. A. Nitric Oxide-Induced Conformational Changes in Soluble Guanylate Cyclase. *Structure* **2014**, 22, 602-611.

(9) Sheff, J. G.; Farshidfar, F.; Bathe, O. F.; Kopciuk, K.; Gentile, F.; Tuszynski, J.; Barakat, K.; Schriemer, D. C. Novel Allosteric Pathway of Eg5 Regulation Identified through Multivariate Statistical Analysis of Hydrogen-Exchange Mass Spectrometry (HX-MS) Ligand Screening Data. *Mol. Cell. Proteomics* **2017**, 16, 428-437.

(10) Donovan, K. A.; Zhu, S. L.; Liuni, P.; Peng, F.; Kessans, S. A.; Wilson, D. J. Conformational Dynamics and Allostery in Pyruvate Kinase. *J. Biol Chem.* **2016**, 291, 9244-9256.

(11) Nussinov, R.; Tsai, C. J. Unraveling structural mechanisms of allosteric drug action. *Trends Pharmacol. Sci.* **2014**, 35, 256-264.

(12) Chen, M. C.; Chen, X.; Schafer, N. P.; Clementi, C.; Komives, E. A.; Ferreiro, D. U.; Wolynes, P. G. Surveying biomolecular frustration at atomic resolution. *Nat. Commun.* **2020**, 11, 9.

(13) Hartl, F. U.; Hayer-Hartl, M. Converging concepts of protein folding *in vitro* and *in vivo*. *Nat. Struct. Mol. Biol.* **2009**, 16, 574-581.

(14) Ma, W.; Schulten, K. Mechanism of Substrate Trans location by a Ring-Shaped ATPase Motor at Millisecond Resolution. *J. Am. Chem. Soc.* **2015**, 137, 3031-3040.

(15) Riback, J. A.; Bowman, M. A.; Zmyslowski, A. M.; Plaxco, K. W.; Clark, P. L.; Sosnick, T. R. Commonly used FRET fluorophores promote collapse of an otherwise disordered protein. *Proc. Natl. Acad. Sci. U. S. A.* **2019**, 116, 8889-8894.

(16) Sekhar, A.; Kay, L. E. NMR paves the way for atomic level descriptions of sparsely populated, transiently formed biomolecular conformers. *Proc. Natl. Acad. Sci. U.S.A.* **2013**.
(17) Hughson, F. M.; Wright, P. E.; Baldwin, R. L. Structural Characterisation of a Partly Folded Apomyoglobin Intermediate. *Science* **1990**, 249, 1544-1548.
(18) Engen, J. R.; Botzanowski, T.; Peterle, D.; Georgescauld, F.; Wales, T. E. Developments in Hydrogen/Deuterium Exchange Mass Spectrometry. *Anal. Chem.* **2021**, 93, 567-582.
(19) Rand, K. D.; Zehl, M.; Jorgensen, T. J. D. Measuring the Hydrogen/Deuterium Exchange of Proteins at High Spatial Resolution by Mass Spectrometry: Overcoming Gas-Phase Hydrogen/Deuterium Scrambling. *Acc. Chem. Res.* **2014**, 47, 3018-3027.
(20) Zheng, J.; Strutzenberg, T.; Pascal, B. D.; Griffin, P. R. Protein dynamics and conformational changes explored by hydrogen/deuterium exchange mass spectrometry. *Curr. Opin. Struct. Biol.* **2019**, 58, 305-313.
(21) Yang, M. L.; Hoeppner, M.; Rey, M.; Kadek, A.; Man, P.; Schriemer, D. C. Recombinant Nepenthesin II for Hydrogen/Deuterium Exchange Mass Spectrometry. *Anal. Chem.* **2015**, 87, 6681-6687.
(22) Wang, G. B.; Kaltashov, I. A. Approach to Characterization of the Higher Order Structure of Disulfide-Containing Proteins Using Hydrogen/Deuterium Exchange and Top-Down Mass Spectrometry. *Anal. Chem.* **2014**, 86, 7293-7298.
(23) Martens, C.; Shekhar, M.; Lau, A. M.; Tajkhorshid, E.; Politis, A. Integrating hydrogen deuterium exchange mass spectrometry with molecular dynamics simulations to probe lipid-modulated conformational changes in membrane proteins. *Nat. Protoc.* **2019**, 14, 3183-3204.
(24) Zhang, Y.; Majumder, E. L. W.; Yue, H.; Blankenship, R. E.; Gross, M. L. Structural Analysis of Diheme Cytochrome c by Hydrogen Deuterium Exchange Mass Spectrometry and Homology Modeling. *Biochemistry* **2014**, 53, 5619-5630.
(25) Hamuro, Y. Tutorial: Chemistry of Hydrogen/Deuterium Exchange Mass Spectrometry. *J. Am. Soc. Mass Spectrom.* **2021**, 32, 133-151.
(26) Habibi, Y.; Uggowitzer, K. A.; Issak, H.; Thibodeaux, C. J. Insights into the Dynamic Structural Properties of a Lanthipeptide Synthetase using Hydrogen-Deuterium Exchange Mass Spectrometry. *J. Am. Chem. Soc.* **2019**, 141, 14661-14672.
(27) Masson, G. R.; Burke, J. E.; Ahn, N. G.; Anand, G. S.; Borchers, C. H.; Brier, S.; Bou-Assaf, G. M.; Engen, J. R.; Englander, S. W.; Faber, J. H.; Garlish, R. A.; Griffin, P. R.; Gross, M. L., et al. Recommendations for performing, interpreting and reporting hydrogen deuterium exchange mass spectrometry (HDX-MS) experiments. *Nat. Methods* **2019**, 16, 595-602.
(28) Vahidi, S.; Bi, Y. M.; Dunn, S. D.; Konermann, L. Load-dependent destabilization of the γ-rotor shaft in FOF1 ATP synthase revealed by hydrogen/deuterium-exchange mass spectrometry. *Proc. Natl. Acad. Sci. U.S.A.* **2016**, 113, 2412-2417.
(29) Maaty, W. S.; Weis, D. D. Label-Free, In-Solution Screening of Peptide Libraries for Binding to Protein Targets Using Hydrogen Exchange Mass Spectrometry. *J. Am. Chem. Soc.* **2016**, 138, 1335-1343.
(30) Hvidt, A.; Nielsen, S. O. Hydrogen exchange in proteins. *Adv. Protein Chem.* **1966**, 21, 287-386.

(31) Craig, P. O.; Lätzer, J.; Weinkam, P.; Hoffman, R. M. B.; Ferreiro, D. U.; Komives, E. A.; Wolynes, P. G. Prediction of native-state hydrogen exchange from perfectly funneled energy landscapes. *J. Am. Chem. Soc.* **2011**, 133, 17463-17472.
(32) Xiao, H.; Hoerner, J. K.; Eyles, S. J.; Dobo, A.; Voigtman, E.; Mel'Cuk, A. I.; Kaltashov, I. A. Mapping protein energy landscapes with amide hydrogen exchange and mass spectrometry: I. A generalized model for a two-state protein and comparison with experiment. *Protein Sci.* **2005**, 14, 543-557.
(33) Persson, F.; Halle, B. How amide hydrogens exchange in native proteins. *Proc. Natl. Acad. Sci. U.S.A.* **2015**, 112, 10383-10388.
(34) Garcia, A. E.; Hummer, G. Conformational dynamics of cytochrome c: Correlation to hydrogen exchange. *Proteins* **1999**, 36, 175-191.
(35) Nishihara, Y.; Kitao, A. Gate-controlled proton diffusion and protonation-induced ratchet motion in the stator of the bacterial flagellar motor. *Proc. Natl. Acad. Sci. U.S.A.* **2015**, 112, 7737-7742.
(36) Fraser, J. S.; van den Bedem, H.; Samelson, A. J.; Lang, P. T.; Holton, J. M.; Echols, N.; Alber, T. Accessing protein conformational ensembles using room-temperature X-ray crystallography. *Proc. Natl. Acad. Sci. U. S. A.* **2011**, 108, 16247-16252.
(37) Amacher, J. F.; Zhong, F. F.; Lisi, G. P.; Zhu, M. Q.; Alden, S. L.; Hoke, K. R.; Madden, D. R.; Pletneva, E. V. A Compact Structure of Cytochrome c Trapped in a Lysine-Ligated State: Loop Refolding and Functional Implications of a Conformational Switch. *J. Am. Chem. Soc.* **2015**, 137, 8435-8449.
(38) Sheu, S. Y.; Yang, D. Y.; Selzle, H. L.; Schlag, E. W. Energetics of hydrogen bonds in peptides. *Proc. Natl. Acad. Sci. U.S.A.* **2003**, 100, 12683-12687.
(39) Weinkam, P.; Zimmermann, J.; Romesberg, F. E.; Wolynes, P. G. The Folding Energy Landscape and Free Energy Excitations of Cytochrome c. *Acc. Chem. Res.* **2010**, 43, 652-660.
(40) Telford, J. R.; Wittung-Stafshede, P.; Gray, H. B.; Winkler, J. R. Protein Folding Triggered by Electron Transfer. *Acc. Chem. Res.* **1998**, 31, 755-763.
(41) Bushnell, G. W.; Louie, G. V.; Brayer, G. D. High-resolution Three-dimensional Structure of Horse Heart Cytochrome c. *J. Mol. Biol.* **1990**, 214, 585-595.
(42) Alvarez-Paggi, D.; Hannibal, L.; Castro, M. A.; Oviedo-Rouco, S.; Demicheli, V.; Tórtora, V.; Tomasina, F.; Radi, R.; Murgida, D. H. Multifunctional Cytochrome c: Learning New Tricks from an Old Dog. *Chem. Rev.* **2017**, 117, 13382-13460.
(43) Yin, V.; Shaw, G. S.; Konermann, L. Cytochrome c as a Peroxidase: Activation of the Pre-Catalytic Native State by H2O2-Induced Covalent Modifications. *J. Am. Chem. Soc.* **2017**, 139, 15701–15709.
(44) Diaz-Quintana, A.; Perez-Mejias, G.; Guerra-Castellano, A.; De la Rosa, M. A.; Diaz-Moreno, I. Wheel and Deal in the Mitochondrial Inner Membranes: The Tale of Cytochrome c and Cardiolipin. *Oxidative Med. Cell. Longev.* **2020**, 2020, 1-20.
(45) Santucci, R.; Sinibaldi, F.; Cozza, P.; Polticelli, F.; Fiorucci, L. Cytochrome c: An extreme multifunctional protein with a key role in cell fate. *Int. J. Biol. Macromol.* **2019**, 136, 1237-1246.
(46) Hannibal, L.; Tomasina, F.; Capdevila, D. A.; Demicheli, V.; Tórtora, V.; Alvarez-Paggi, D.; Jemmerson, R.; Murgida, D. H.; Radi, R. Alternative Conformations of Cytochrome c: Structure, Function, and Detection. *Biochemistry* **2016**, 55, 407-428.

(47) Gu, J.; Shin, D.-W.; Pletneva, E. V. Remote Perturbations in Tertiary Contacts Trigger Ligation of Lysine to the Heme Iron in Cytochrome c. *Biochemistry* **2017**, 56, 2950−2966.
(48) Dharmasiri, K.; Smith, D. L. Regional Stability Changes in Oxidized and Reduced Cytochrome c Located by Hydrogen Exchange and Mass Spectrometry. *J. Am. Soc. Mass Spectrom.* **1997**, 8, 1039-1045.
(49) Rovira, C.; Carloni, P.; Parrinello, M. The iron-sulfur bond in cytochrome c. *J. Phys. Chem. B* **1999**, 103, 7031-7035.
(50) Trewhella, J.; Carlson, V. A. P.; Curtis, E. H.; Heidorn, D. B. Differences in the Solution Structures of Oxidized and Reduced Cytochrome c Measured by Small-Angle X-ray Scattering. *Biochemistry* **1988**, 27, 1121-1125.
(51) Banci, L.; Bertini, I.; Huber, J. G.; Spyroulias, G. A.; Turano, P. Solution structure of reduced horse heart cytochrome c. *J. Biol. Inorg. Chem.* **1999**, 4, 21-31.
(52) Tezcan, F. A.; Winkler, J. R.; Gray, H. B. Effects of Ligation and Folding on Reduction Potentials of Heme Proteins. *J. Am. Chem. Soc.* **1998**, 120, 13383-13388.
(53) Xu, Y.; Mayne, L.; Englander, S. W. Evidence for an unfolding and refolding pathway in cytochrome *c*. *Nat. Struct. Biol.* **1998**, 5, 774-778.
(54) Reinhard, M. E.; Mara, M. W.; Kroll, T.; Lim, H.; Hadt, R. G.; Alonso-Mori, R.; Chollet, M.; Glownia, J. M.; Nelson, S.; Sokaras, D.; Kunnus, K.; van Driel, T. B.; Hartsock, R. W., et al. Short-lived metal-centered excited state initiates iron-methionine photodissociation in ferrous cytochrome c. *Nat. Commun.* **2021**, 12, 1086-1086.
(55) Ascenzi, P.; Coletta, M.; Santucci, R.; Polizio, F.; Desideri, A. Nitric-oxide binding to ferrous native horse heart cytochrome-c and to its carboxymethylated derivative - a spectroscopic and thermodynamic study. *J. Inorg. Biochem.* **1994**, 53, 273-280.
(56) Yoshimura, T.; Suzuki, S. The ph-dependence of the stereochemistry around the heme group in no cytochrome-c (horse heart). *Inorg. Chim. Acta* **1988**, 152, 241-249.
(57) Jones, C. M.; Henry, E. R.; Hu, Y.; Chan, C.; Luck, S. D.; Bhuyan, A.; Roder, H.; Hofrichter, J.; Eaton, W. A. Fast events in protein folding initiated by nanosecond laser photolysis. *Proc. Natl. Acad. Sci. U.S.A.* **1993**, 90, 11860-11864.
(58) Fedurco, M.; Augustynski, J.; Indiani, C.; Smulevich, G.; Antalik, M.; Bano, M.; Sedlak, E.; Glascock, M. C.; Dawson, J. H. The heme iron coordination of unfolded ferric and ferrous cytochrome c in neutral and acidic urea solutions. Spectroscopic and electrochemical studies. *BBA-Proteins Proteomics* **2004**, 1703, 31-41.
(59) Indiani, C.; de Sanctis, G.; Neri, F.; Santos, H.; Smulevich, G.; Coletta, M. Effect of pH on axial ligand coordination of cytochrome c " from Methylophilus methylotrophus and horse heart cytochrome c. *Biochemistry* **2000**, 39, 8234-8242.
(60) Battistuzzi, G.; Bortolotti, C. A.; Bellei, M.; Di Rocco, G.; Salewski, J.; Hildebrandt, P.; Sola, M. Role of Met80 and Tyr67 in the Low-pH Conformational Equilibria of Cytochrome c. *Biochemistry* **2012**, 51, 5967-5978.
(61) Arcovito, A.; Gianni, S.; Brunori, M.; Travaglini-Allocatelli, C. Fast Coordination Changes in Cytochrome c Do Not Necessarily Imply Folding. *J. Biol. Chem.* **2001**, 276, 41073-41078.
(62) Abraham, M. J.; Murtola, T.; Schulz, R.; Páll, S.; Smith, J. C.; Hess, B.; Lindahl, E. GROMACS: High performance molecular simulations through multi-level parallelism from laptops to supercomputers. *SoftwareX* **2015**, 1–2, 19-25.
(63) Huang, J.; MacKerell, A. D. CHARMM36 all-atom additive protein force field: Validation based on comparison to NMR data. *J. Comput. Chem.* **2013**, 34, 2135-2145.

(64) Marmorino, J. L.; Auld, D. S.; Betz, S. F.; Doyle, D. F.; Young, G. B.; Pielak, G. J. Amide proton exchange rates of oxidized and reduced Saccharomyces cerevisiae iso-1-cytochrome c. *Protein Science* **1993**, 2, 1966-1974.
(65) Mohammadiarani, H.; Shaw, V. S.; Neubig, R. R.; Vashisth, H. Interpreting Hydrogen-Deuterium Exchange Events in Proteins Using Atomistic Simulations: Case Studies on Regulators of G-Protein Signaling Proteins. *J. Phys. Chem. B* **2018**, 122, 9314-9323.
(66) Narang, D.; Chen, W.; Ricci, C. G.; Komives, E. A. RelA-Containing NF kappa B Dimers Have Strikingly Different DNA-Binding Cavities in the Absence of DNA. *J. Mol. Biol.* **2018**, 430, 1510-1520.
(67) Skinner, J. J.; Yu, W.; Gichana, E. K.; Baxa, M. C.; Hinshaw, J. R.; Freed, K. F.; Sosnick, T. R. Benchmarking all-atom simulations using hydrogen exchange. *Proc. Natl. Acad. Sci. U.S.A.* **2014**, 111, 15975-15980.
(68) McAllister, R. G.; Konermann, L. Challenges in the Interpretation of Protein H/D Exchange Data: A Molecular Dynamics Simulation Perspective. *Biochemistry* **2015**, 54, 2683-2692.
(69) Piana, S.; Lindorff-Larsen, K.; Shaw, D. E. Atomic-level description of ubiquitin folding. *Proc. Natl. Acad. Sci. U.S.A.* **2013**, 110, 5915-5920.
(70) Banci, L.; Bertini, I.; Bren, K. L.; Gray, H. B.; Sompornpisut, P.; Turano, P. Three-Dimensional Solution Structure of the Cyanide Adduct of a Met80Ala Variant of Saccharomyces cerevisiae Iso-1-cytochrome c. Identification of Ligand—Residue Interactions in the Distal Heme Cavity1. *Biochemistry* **1995**, 34, 11385-11398.
(71) Ciaccio, C.; Tognaccini, L.; Battista, T.; Cervelli, M.; Howes, B. D.; Santucci, R.; Coletta, M.; Mariottini, P.; Smulevich, G.; Fiorucci, L. The Met80Ala and Tyr67His/Met80Ala mutants of human cytochrome c shed light on the reciprocal role of Met80 and Tyr67 in regulating ligand access into the heme pocket. *J. Inorg. Biochem.* **2017**, 169, 86-96.
(72) Torshin, I. Y.; Weber, I. T.; Harrison, R. W. Geometric criteria of hydrogen bonds in proteins and identification of 'bifurcated' hydrogen bonds. *Protein Eng.* **2002**, 15, 359-363.
(73) Wand, A. J.; Roder, H.; Englander, S. W. Two-dimensional 1H NMR studies of cytochrome c: hydrogen exchange in the N-terminal helix. *Biochemistry* **1986**, 25, 1107-1114.
(74) Skoog, D. A.; Holler, F. J.; Nieman, T. A. *Principles of Instrumental Analysis*; Harcourt Brace College Publishers: Philadelphia, PA, 1998.

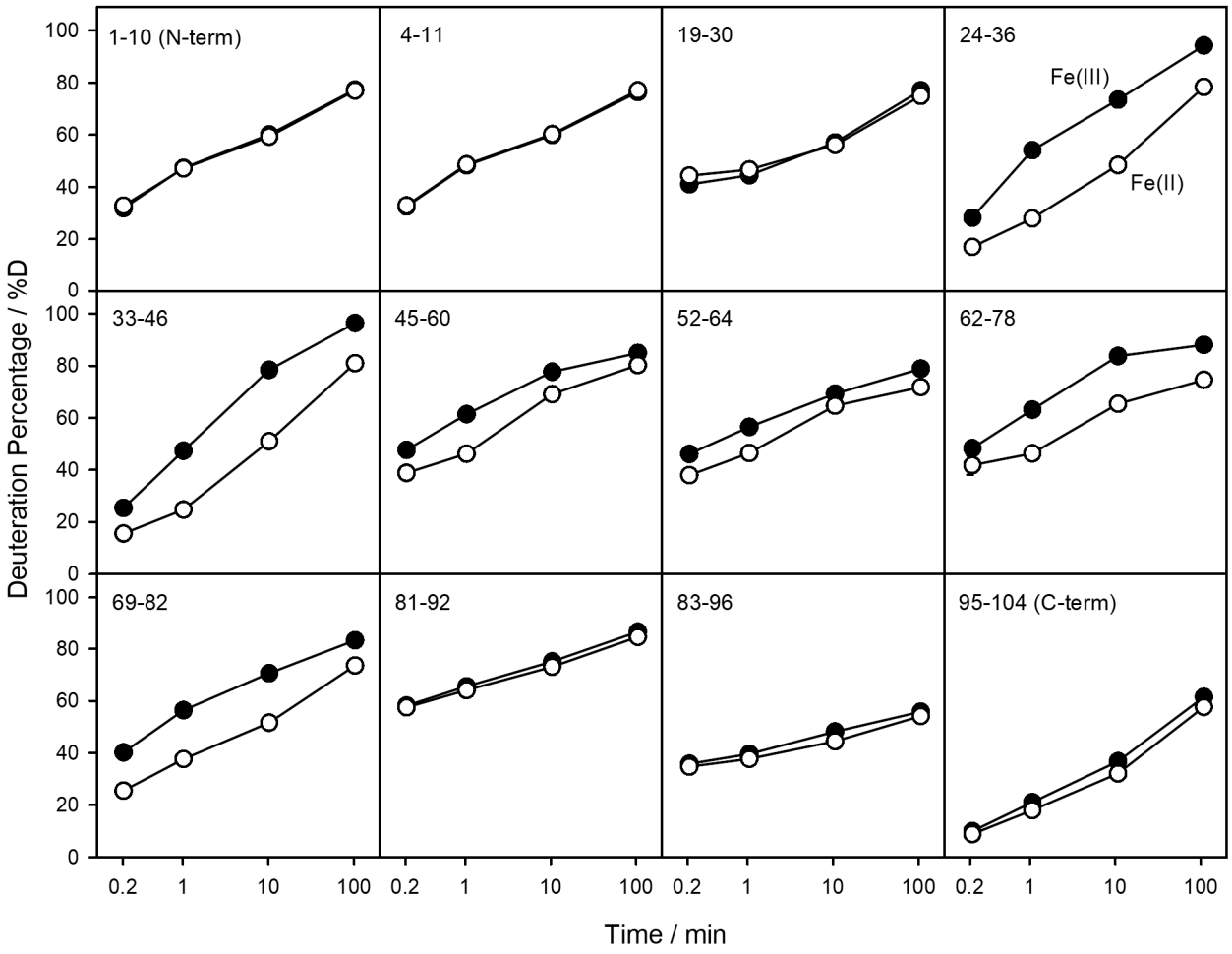

Figure 1. Experimental HDX uptake for selected peptides in Fe(III) (●) and Fe(II) (○) cyt *c*. The data shown are the results of triplicate measurements. Error bars are smaller than the symbol size.

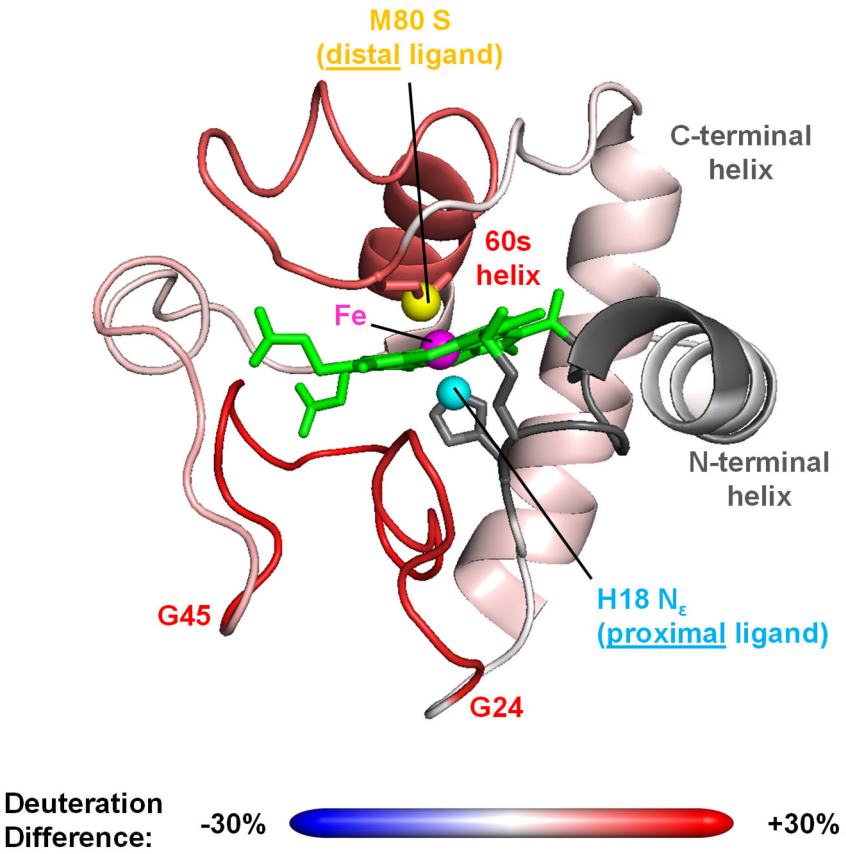

Figure 2. HDX difference plot ($\%D_{Fe(III)} - \%D_{Fe(II)}$) superimposed onto the cyt *c* crystal structure[41] using data from Figure 1 for $t = 10$ min. Segments where the Fe(III) state shows higher deuteration than the Fe(II) state appear in red. Heme is depicted in green, distal/proximal ligating atoms of the heme Fe are highlighted as spheres. The protein forms three major α helices (N-terminal, 60s, and C-terminal), and three Ω loops that cover residues 18-36, 40-57 and 71-85.[2]

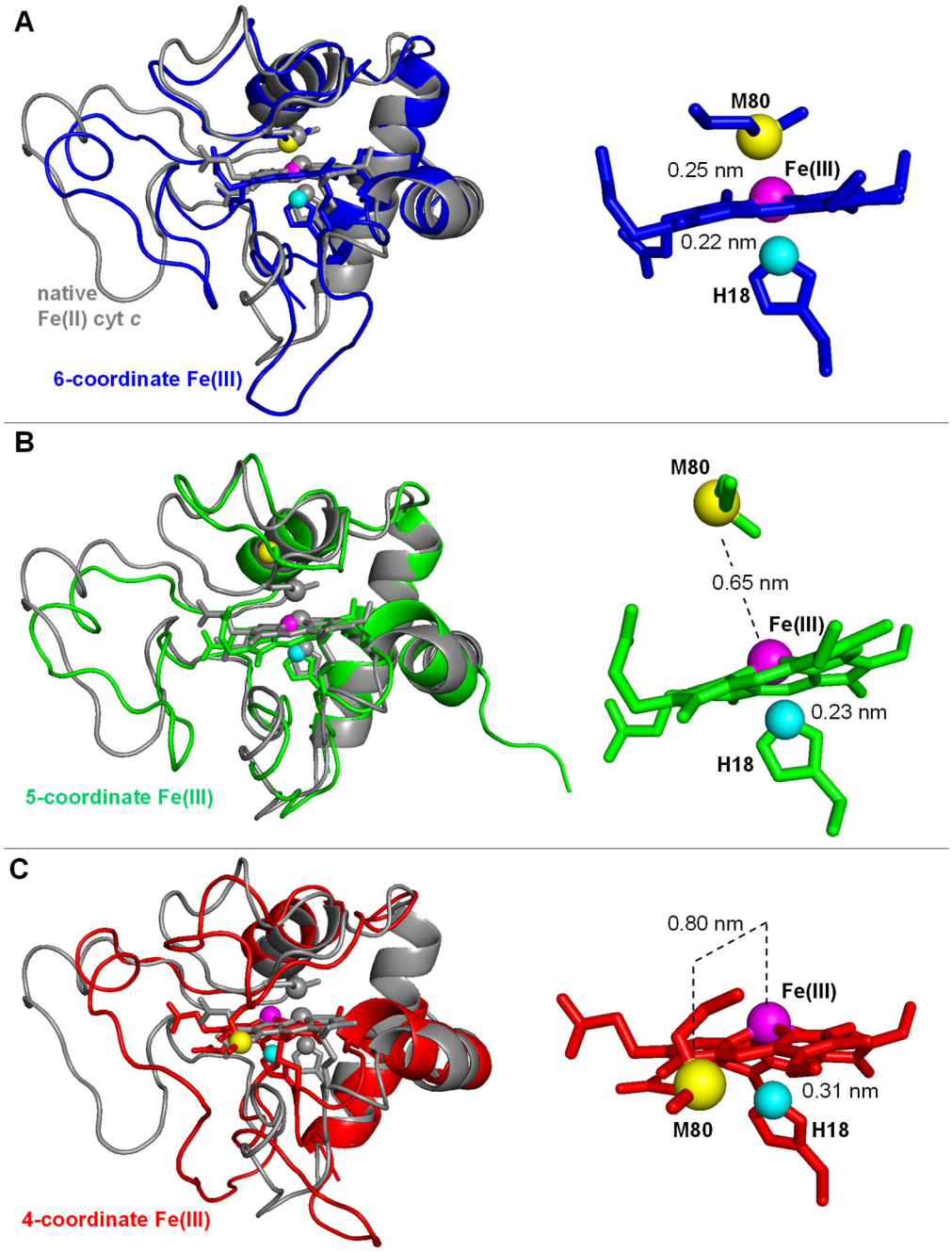

Figure 3. MD structures for different ligation scenarios. (A) Blue: 6-coordinate Fe(III) cyt *c*, (B) green: 5-coordinate Fe(III) cyt *c*, (C) red: 4-coordinate Fe(III) cyt *c*. Panels on the left also show native Fe(II) cyt *c* as reference (gray). Panels on the right highlight heme, M80, and H18, along with the corresponding S/Fe and Fe/N_{ε} distances. The data shown here represent time points around 500 ns taken from 1 μs MD trajectories.

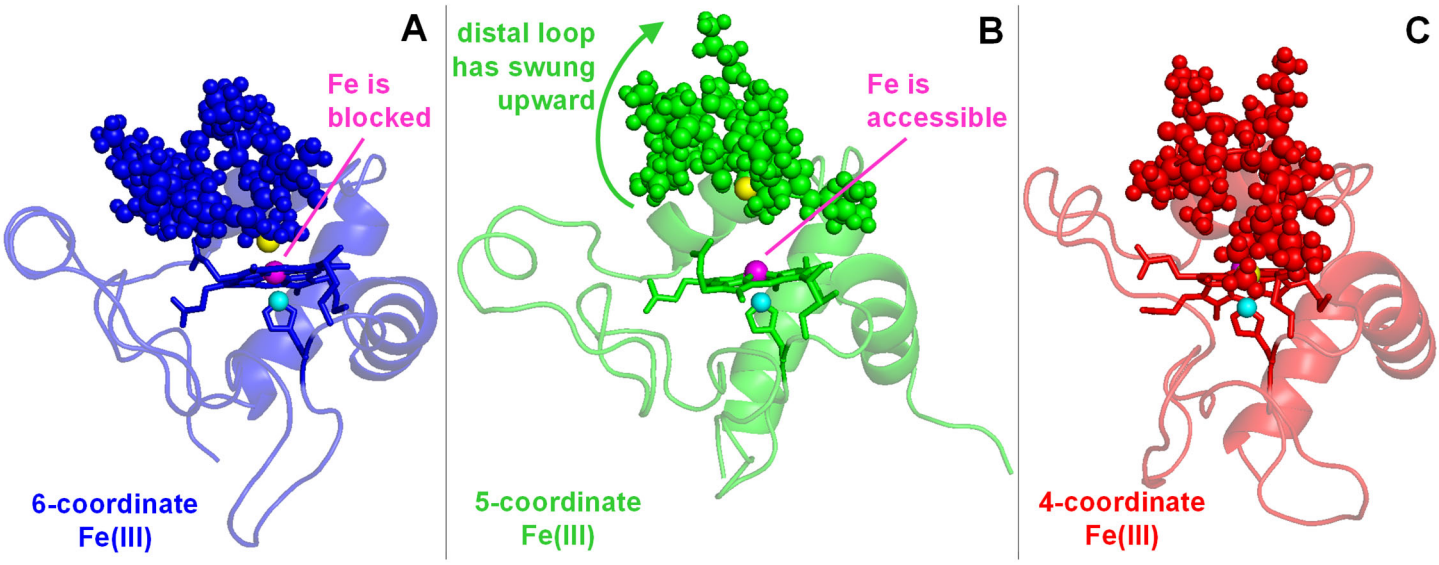

Figure 4. Comparison of Fe(III) species with focus on the distal Ω loop. Residues 71-81 of the loop are shown in spacefill representation. These are the same MD structures as in Figure 3, but in a different orientation. (A) 6-coordinate, (B) 5-coordinate, (C) 4-coordinate Fe(III) cyt *c*. Heme iron is magenta, M80 S is yellow, H18 N_{ε} is cyan.

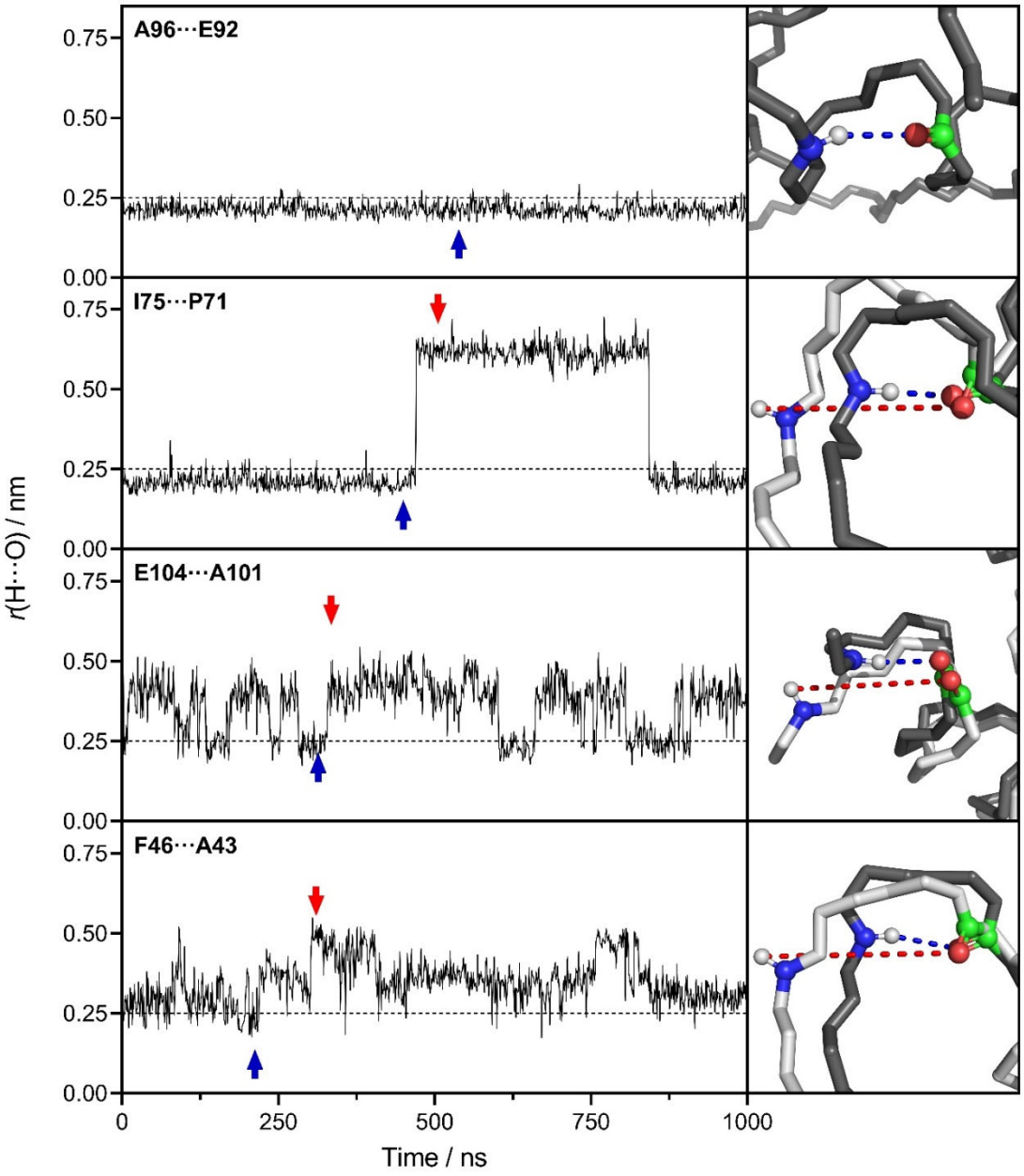

Figure 5. MD simulation data, exemplifying H-bond dynamics for different NH···OC contacts in 6-coordinate Fe(III) cyt *c*. For each pair the NH donor is listed first. Panels on the left show hydrogen-oxygen distances vs. time. Vertical dotted lines at 0.25 nm indicate the H-bond cut-off. The top panel illustrates an H-bond that is permanently closed. All others undergo $NH_{CLOSED} \leftrightarrow NH_{OPEN}$ transitions. Panels on the right illustrate MD snapshots as overlays of NH_{CLOSED} (blue dashed) and NH_{OPEN} (red dashed) conformers, for time points indicated by the blue and red arrows. Element coloring: N (blue), H (white), O (red), C (green).

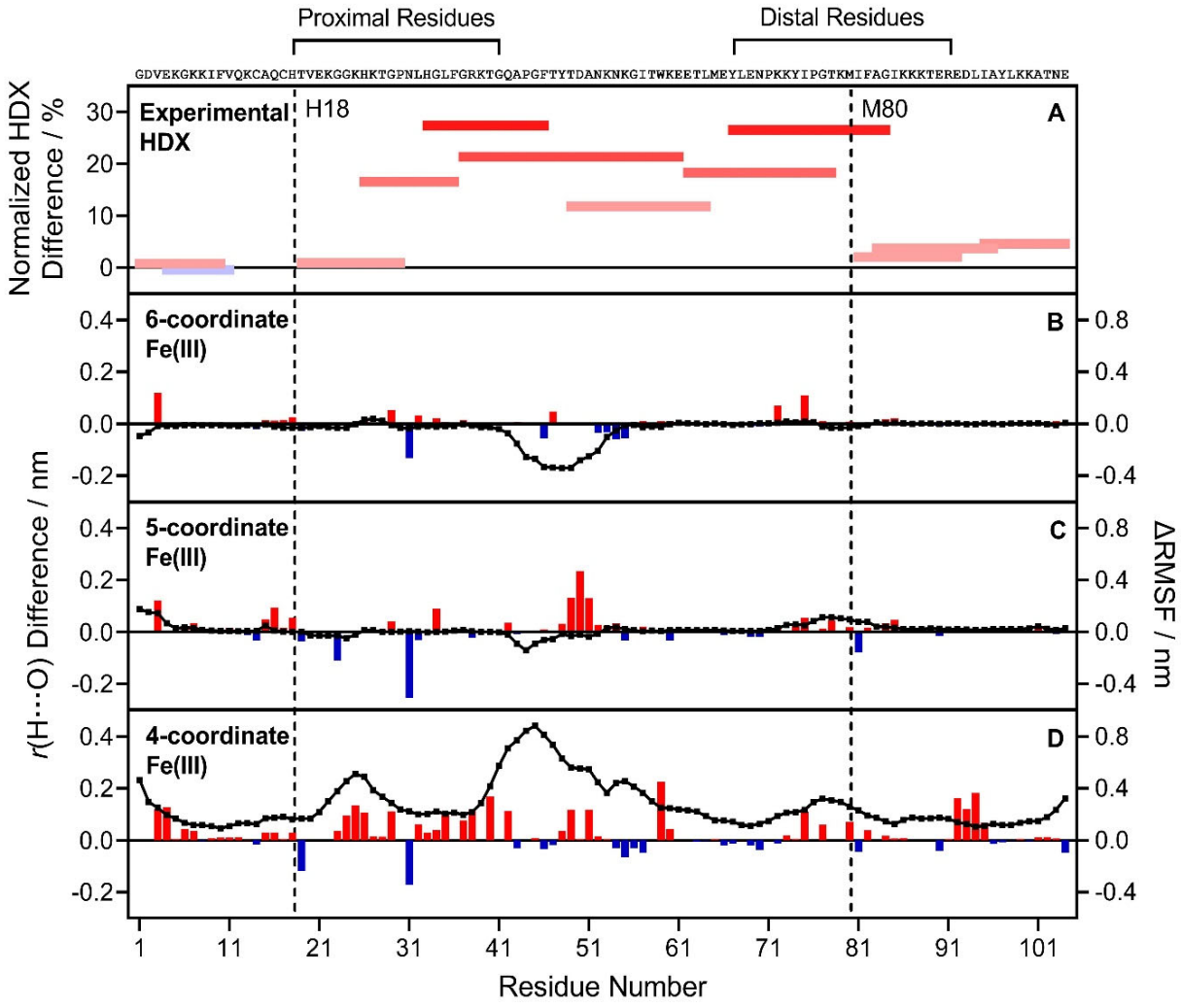

Figure 6. Fe(III) – Fe(II) difference plots. (A) Experimental HDX data for t = 10 min. Positive (red) indicates where Fe(III) is more highly deuterated than native Fe(II) cyt *c*. The other panels show MD data. (B) Difference plot for 6-coordinate Fe(III), (C) difference plot for 5-coordinate Fe(III), (D) difference plot for 4-coordinate Fe(III). Vertical bars in B-D represent NH···OC contacts that are more open (red) or more closed (blue) than in native Fe(II) cyt *c*. ΔRMSF for backbone N atoms are shown in black; ΔRMSF > 0 indicates where Fe(III) fluctuates more, ΔRMSF < 0 indicates where Fe(III) fluctuates less than native Fe(II) cyt *c*.

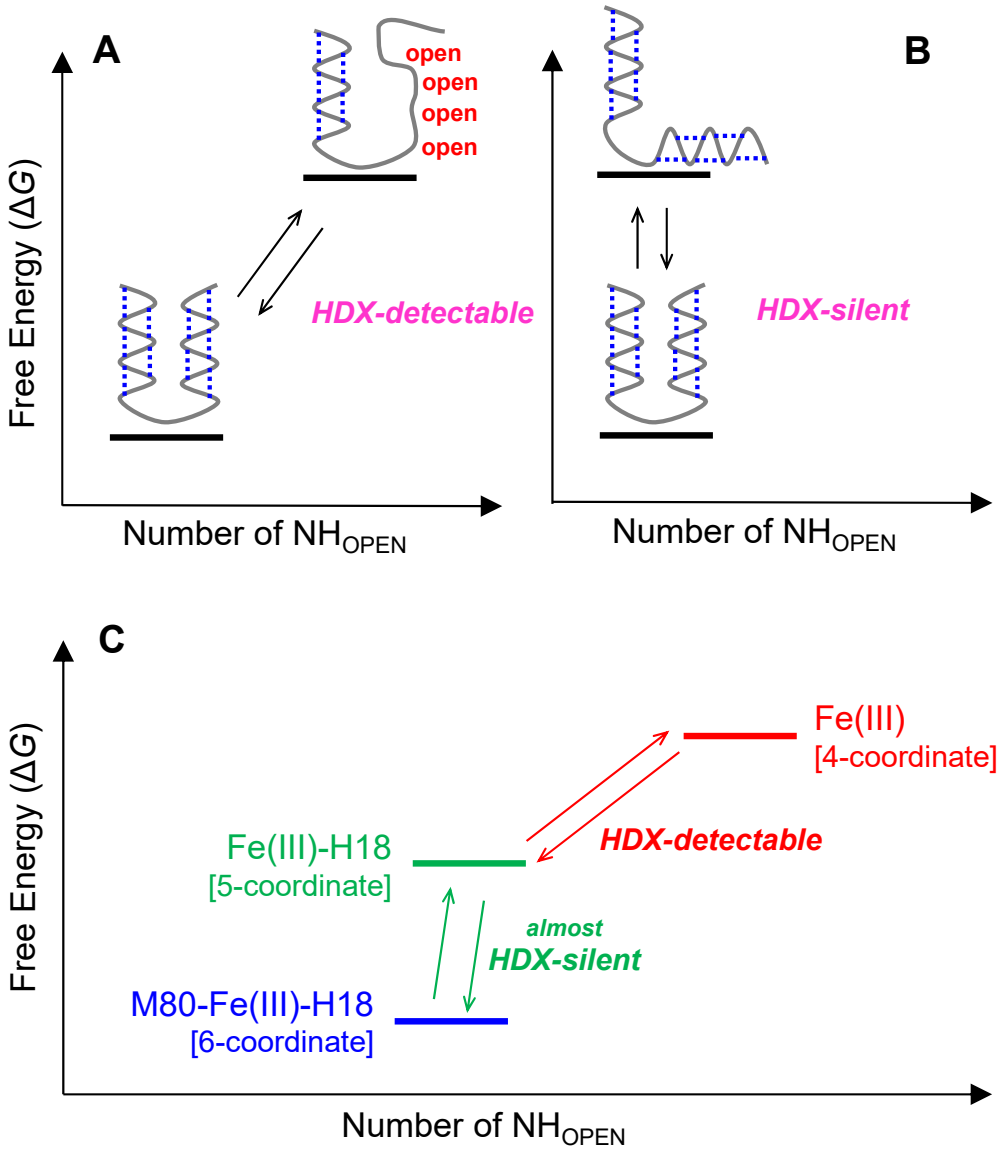

Figure 7. Cartoon of protein fluctuations between Boltzmann-populated states. (A) HDX-detectable scenario, where two conformers differ in the number of NH$_{OPEN}$ sites. (B) HDX-silent scenario, where two conformers share the same H-bond pattern. Blue dotted lines indicate "closed" H-bonds. (C) Dynamics that are enhanced in Fe(III) cyt *c* relative to the Fe(II) protein. Fluctuations between 6/5-coordinate cyt *c* occur with very minor changes in H-bonding. Fluctuations between 5/4-coordinate cyt *c* are associated with major H-bond opening/closing (see Figure 4).

Table of Contents Figure